Optical determination of solid fat content in fats and oils: effects of wavelength on estimated accuracy

Optical Determination of Solid Fat Content in Fats and Oils: Effects of Wavelength on Estimated Accuracy

Marco Grossi[a], Enrico Valli[b,c], Virginia Teresa Glicerina[c], Pietro Rocculi[c], Tullia Gallina Toschi[b,c], Bruno Riccò[a]

Corresponding author: marco.grossi8@unibo.it , Tel. 0039-0512093038

[a] Department of Electrical Energy and Information Engineering "Guglielmo Marconi" (DEI), *Alma Mater Studiorum*, University of Bologna, Bologna, Italy

[b] Department of Agricultural and Food Sciences (DISTAL), *Alma Mater Studiorum*, University of Bologna, Cesena, Italy

[c] Interdepartmental Centre of Agri-food Industrial Research (CIRI Agroalimentare), *Alma Mater Studiorum*, University of Bologna, Cesena, Italy

Abstract

The melting profile of solid fat content (SFC) is a parameter of primary importance for the food industry since it affects many important product characteristics such as stability, physical appearance, spreadability, and sensation in the mouth. Reference techniques to measure SFC in fats and oils include pulsed nuclear magnetic resonance (pNMR) and differential scanning calorimetry (DSC), which are reliable and accurate, but require expensive instrumentation and trained personnel. Herein, the accuracy of a recently proposed optical technique to measure SFC was investigated in terms of peak wavelength of incident radiation. A sensor system featuring an array of seven LEDs with peak wavelength in the visible and NIR range was built, and the results compared with data from DSC. All the wavelengths investigated had high accuracy in SFC estimation, especially at 590 nm (yellow) and 880 nm (NIR).

Practical applications

Quick and easy determination of solid fat content in fats and oils by a simple experimental setup. The technique is based on optical attenuation measurements during a thermal cycle. The technique can be implemented in a measurement instrument for in-situ analysis of solid fat content.

Keywords: solid fat content, optical sensor, food analysis, phase transition, embedded systems.

1. Introduction

The solid fat content (SFC) of fats and oils is an important parameter for many properties of food products including physical appearance, organoleptic and rheological properties, spreadability, and plasticity [1]. In particular, the melting profile (i.e. SFC variation with temperature) is very important since many of the characteristics of the product are affected by this parameter and specific requirements must be met [2]. For example, SFC values in the range from 4 to 10 °C determine the ease of spreading at refrigeration temperature, values from 20 to 22 °C determine the product's stability and resistance to oil exudation at room temperature, and values from 33 to 38 °C influence how the product feels in the mouth induced by the fat [1].

The official method according to ISO standard for determination of SFC is pulsed nuclear magnetic resonance (pNMR) [3], which is widely used in the food industry [4]. However, pNMR requires expensive instrumentation, and measurements by this method must be performed at fixed temperatures. Differential scanning calorimetry (DSC) is an alternative technique that can provide a melting profile of the product that is easy to perform and generally provides reproducible results [5, 6]. Other techniques have also been proposed for

determination of SFC, such as Fourier transform near-infrared (FT-NIR) spectroscopy [7] and ultrasonic velocimetry [8].

The techniques used for the determination of SFC are reliable, but must be implemented in a laboratory environment and require trained personnel. Thus, in the case of small and medium food industries, which cannot afford an internal laboratory for quality control, the only choice is to rely on an external laboratory. This leads to higher costs for analysis, and may cause a non-negligible delay between delivery of samples and results of the analysis.

On the other hand, portable embedded sensor systems based on microcontrollers, field programmable gate arrays (FPGAs) or modern smartphones, are very attractive since they can carry out *in-situ* measurements using less expensive electronics, thus providing near real-time results at very low cost, making this technique rapid and affordable for small food industries. Some examples of sensors and sensor systems recently proposed in the literature for food analysis include evaluation of the microbial content in raw milk [9]; real-time detection of bovine milk adulteration [10]; estimation of fish freshness using impedance sensors [11]; characterization and control of ice cream properties with electrical impedance [12, 13]; detection of freshness of chicken meat [14]; assessment of lycopene content in tomatoes [15]; detection of bacterial contamination in meat [16]; quality analysis of olive oil [17, 18, 19]; rapid non-destructive testing of fruit firmness [20]; low-cost analysis of edible oil oxidation using electrical conductivity measurements [21]; handheld near-infrared spectroscopy analysis for characterization of extra virgin olive oil [22].

A technique to estimate SFC in fats and oils, based on single wavelength (near-infrared) optical measurements during a thermal cycle, has been previously developed [23]. The proposed method is simple and accurate, and can be easily used as a low-cost electronic embedded system for *in-situ* measurements of SFC. Herein, we investigated the effects of LED wavelength on the accuracy of the estimated SFC. Towards this end, an optical sensor system featuring an array of seven LEDs and a photodiode was used to make optical

attenuation measurements at different wavelengths (in the visible and near-infrared region) during a thermal cycle (heating and cooling). Several wavelengths were investigated to provide the most accurate estimation of SFC.

2. Experimental Approach

The overall aim was to develop an embedded sensor system for in-situ SFC measurements of fats and oils in an industrial setting. Accordingly, it was important to design the system using low-cost electronics and, at the same time, to guarantee high accuracy compared with the reference technique. Previous studies have examined the SFC of food products using visible and NIR spectroscopy [24][25]. These techniques estimate SFC from a broad visible/NIR optical spectrum using a commercial spectrometer and chemometric analysis. However, a commercial spectrometer is an expensive instrument that performs measurements at a single temperature. Thus, we developed a simple, low-cost sensor that integrates seven LEDs and measures optical attenuation at seven discrete wavelengths in the UV/visible/NIR region. The seven LEDs cover the wavelength range 395–880 nm, since in this region low-cost solutions are available for integrated electronics (LEDs, photodiode) and sample containers. Optical attenuation measurements were carried out using the *ad-hoc* multi-wavelength optical sensor placed in a thermal chamber (Binder APT KB 53). Tests were carried out on a set of 16 fats and oils, which included cocoa butter, shea butter, hydrogenated soybean oil, and refined and fractionated coconut oils, as well as various blends (Table 1). In the present investigations, measurements were made by placing the sensor in a thermal chamber, and the measured data (optical and temperature) were transferred from the microcontroller to a computer for analysis and calculation of SFC. The system has the potential to be completely autonomous where the thermal cycle is implemented with an ad-hoc designed thermal chamber based on Peltier cells (controlled by an additional electronic board), with all data analyses carried out by the microcontroller. This allows for the development of a completely portable sensor system that,

in contrast to reference techniques for measurement of SFC (pNMR and DSC), can perform measurements in-the-field.

Optical data were used to estimate the SFC and the accuracy was compared with that obtained by DSC. DSC measurements were carried out using a DSC Q20 (TA Instruments, USA) as described by Lopez et al. in 2006 [26].

2.1 Sensor System

The *ad-hoc* built sensor system used is shown in Fig. 1. It was designed using the software Solid Edge v17 and built with a 3D printer (MakerBot Replicator Z18). The system is composed of a drawer with a glass slide (75 mm x 25 mm) featuring a spherically polished cavity (diameter 13 mm, depth 0.3 mm). The sample under test (SUT) is hosted in this cavity during measurements. At the bottom of the system, an array of seven LEDs with different wavelengths is present: 395 nm (UV), 468 nm (blue), 523 nm (green), 590 nm (yellow), 610 nm (amber), 630 nm (red), and 880 nm (infrared). On the top of the system, a photodiode (BPW20RF by Vishay) with wavelength sensitivity between 380 nm and 1000 nm is present that collects the radiation generated by the LEDs and transmits it through the SUT.

The schematics of the electronic board used to control the LEDs and measure the photodiode current are also shown in Fig. 1. This board is based on the microcontroller STM32L152RE from ST Microelectronics and transfers data to a laptop PC using serial communication via LabVIEW programs (National Instruments, USA). The seven LEDs are driven by the integrated circuit TLC5916 (Texas Instruments, USA), a constant current LED driver capable to support a maximum of eight LEDs, and controlled by a microcontroller using the Serial Peripheral Interface (SPI) port. The photodiode collects the incident radiation and generates a current (I_{PHOTO}) that is converted to a voltage V_{OUT} by a current to voltage (I/V) converter (with a feedback resistance of 56 kΩ), followed by a non-inverting amplifier. The output voltage V_{OUT} can be calculated as:

$$V_{OUT} = \left(R_A \cdot I_{PHOTO}\right) \cdot \left(1 + \frac{R_F}{R_B}\right), \quad (1)$$

where R_A = 56 kΩ, R_B = 1 kΩ, while R_F is the resistance of the programmable digital potentiometer MCP4131 (127 steps in the range 0 – 10 kΩ) that is controlled by the microcontroller SPI port. The voltage V_{OUT} is acquired with the 12-bits ADC of the microcontroller.

A negative temperature coefficient (NTC) temperature sensor (B57045K by TDK), placed near the SUT, is used to measure the SUT temperature. The temperature sensor is used in a voltage divider, as shown in Fig. 1. The corresponding voltage V_{TEMP} is acquired by the microcontroller ADC and the temperature is calculated by the microcontroller.

2.2 Measurement Technique

The SUT in the sensor system can be hosted, from an optical point of view, as shown in Fig. 2a. The radiation generated by the LED (I_{IN}) travels through the sample (composed of a solid and a liquid phase) and is attenuated by absorption and scattering, as well as by the reflections at different interfaces. With reference to Fig. 2 (a), d_1 and d_2, these refer to the thickness of the solid and liquid phase and α_s and α_l are the attenuation coefficients for the solid and liquid phase; τ_0, τ_1, and τ_2 are the transmission coefficients for the glass/solid phase interface, solid/liquid phase interface, and liquid/air interface, respectively. The output radiation (I_{OUT}) can be expressed as a function of the input radiation (I_{IN}) with the equation:

$$\frac{I_{OUT}}{I_{IN}} = \tau_2 \cdot \tau_1 \cdot \tau_0 \cdot e^{-\alpha_s \cdot d_1 - \alpha_l \cdot d_2}, \quad (2)$$

The sensor system was placed in a thermal chamber (Binder APT KB 53) and subjected to the thermal cycle shown in Fig. 2b: the temperature first was set to T_{HIGH} (75 °C) for 60 minutes; next, a cooling cycle was carried out by changing the temperature from T_{HIGH} to T_{LOW} (−15 °C) at −0.5 °C/min; T_{LOW} was then maintained for 10 minutes; finally, a heating cycle was carried out by changing the temperature from T_{LOW} to T_{HIGH} at 0.5 °C/min. The logarithm of

the acquired voltage V_{OUT}, normalized between 0 and 100, (hereafter referred to as the output value) was saved for both the cooling and heating cycles for all samples at the seven wavelengths investigated.

The sample SFC *vs* temperature curve was estimated using the measured optical data with the algorithm presented in [23].

1) For each wavelength and sample, two parameters were extracted from the optical thermogram. As presented in Fig. 3 in the case of the infrared LED and sample 8 in Table 1, the temperatures resulting in 90% of the total variation of the output value during the cooling ($T_{90\%,COOLING}$) and heating cycles ($T_{90\%,HEATING}$). The calculated values of the parameters $T_{90\%,COOLING}$ and $T_{90\%,HEATING}$ are shown in Table 2 for all samples and wavelengths.

2) The temperatures at which SFC determined by DSC is 10% ($T_{10\%,DSC}$) and 90% ($T_{90\%,DSC}$) were estimated by a linear model defined by the following equations:

$$T_{90\%,DSC} = \beta_1 + \beta_2 \cdot T_{90\%,COOLING} + \beta_3 \cdot T_{90\%,HEATING}, \quad (3)$$

$$T_{10\%,DSC} = \beta_4 + \beta_5 \cdot T_{90\%,COOLING} + \beta_6 \cdot T_{90\%,HEATING}, \quad (4)$$

The parameters β_1, β_2, β_3, β_4, β_5, and β_6 were estimated by carrying out a multiple linear regression analysis on the set of 16 samples where $T_{90\%,DSC}$ and $T_{10\%,DSC}$ are the independent variables extracted from the DSC thermogram, while $T_{90\%,COOLING}$ and $T_{90\%,HEATING}$ are the dependent variables extracted from the optical thermogram and reported in Table 2. Multiple regression analysis was carried out for each wavelength investigated. The model parameters are presented in Table 3.

3) The thermogram (SFC *vs* temperature) was estimated by using a sigmoidal model (Ratkowsky model) defined as:

$$SFC = \frac{100}{1 + e^{b - c \cdot T}}, \quad (5)$$

where T is expressed in Kelvin and the empirical parameters (b and c) were determined by the estimated values of $T_{90\%,DSC}$ and $T_{10\%,DSC}$ using the equations:

$$c = \frac{2 \cdot \ln(9)}{T_{90\%,DSC} - T_{10\%,DSC}}, \quad (6)$$

$$b = \ln(9) + c \cdot T_{10\%,DSC}. \quad (7)$$

2.3. Statistical Analysis

The performance of the method was estimated by using the indicator of mean square error (MSE), which gives information on the mean quadratic discrepancy between the target values and the predicted ones. MSE can be defined by the following equation:

$$MSE = \frac{1}{N} \cdot \sum_{i=1}^{N} (Y_i - X_i)^2, \quad (8)$$

where N = 16 is the number of samples, and Y_i and X_i are the temperatures corresponding to a particular value of SFC determined by the estimated SFC thermogram and DSC data, respectively. Low values of MSE result in better accuracy for the estimated SFC.

3. Results and discussion

A typical thermogram curve (SFC *vs* temperature) obtained by DSC is shown in Fig. 4a, while the measured output value *vs* temperatures is presented, for all wavelengths investigated, in Fig. 4b for the cooling cycle and in Fig. 4c for the heating cycle. In all three cases, sample 8 in Table 1 is presented as an example. The thermograms for the other samples had a similar curve with different temperature ranges (Table 2). As can be seen, all wavelengths result in similar curves with the yellow (590 nm) and NIR (880 nm) LEDs producing higher output values during the melting/solidification of the sample.

SFC estimation using the different LEDs was evaluated by determining the SFC thermogram for each sample using the technique described in Section 2, i.e. equations 5, 6, and 7, and then comparing the estimated temperatures at which SFC is 80%, 60%, 40%, and 20%, in agreement with Grossi et al., 2020 [23], using the proposed optical approach and DSC. All the wavelengths investigated resulted in high accuracy for the estimated SFC. The accuracy was

evaluated by calculating the MSE, in agreement with Goverin et al. (2009) who assessed the potentiality of Raman spectroscopy to predict the SFC of an anhydrous milk fat; Mehrban et al. (2017) compared the performances of different genomic selection methods using this parameter and Florent-Felizaz et al. (2021) used MSE to estimate the capacity of image analysis of conventional magnetic resonance to predict the results obtained from quantitative MRI [27, 28, 29].

Values of MSE were calculated for SFC at 80%, 60%, 40%, and 20% for all investigated wavelengths (Fig. 5), and the results for all wavelengths were highly accurate. However, the NIR LED (880 nm) produced the best results for SFC 80% and 20%, while the yellow LED (590 nm) had slightly better accuracy than the NIR LED for SFC 60% and 40%, demonstrating a greater capacity to predict SFC in a wider range of temperatures than those with NMR. The results showed high correlations between selected NIR wavelengths and DSC measurements at both low and high temperatures [30,31,32]. Moreover, as reported by several authors, the high predictive ability obtained in our study at both low and high temperatures compared to studies with NMR, even in comparison with those using NIR, can be probably attributed to the discrepancy between NMR and DSC. The reported differences in SFC between the NMR and DSC can likely be attributed to the fact that DSC is based on melting energy, which is the not the same as actual melted mass, since the consumed energy per unit of melted mass tends to increase with the increase in melting temperature of each fraction of the fat. In this regard, corrections have been proposed to estimate the melted mass from melting energy, which provides results that are much closer to those obtained with NMR [5]. DSC is a dynamic technique in which SFC values are obtained by measuring the melting enthalpies of fats that characterizes the entire melting process, while NMR is a static analysis based on the evaluation of the relative amount of protons present in triglycerides. As described in the literature, the variation in heat of fusion is normally greater than the corresponding variation in the amount of protons, and for this reason the latter method can

give rise to low and underestimated values, especially at lower temperatures [30, 31, 33, 34, 35, 36].

Fig. 6 shows the scatter plots for the temperature estimated from optical and DSC data for SFC = 80% (a), 60% (b), 40% (c), and 20% (d) with the NIR LED. As can be seen, there is high correlation between estimated values and data from DSC with a coefficient of determination R^2 that is not lower than 0.89. Results for all the wavelengths investigated are presented in Table 4, which confirm the results with the NIR wavelength (880 nm); better results are seen for SFC values of 80% and 20%, while the yellow wavelength (590 nm) shows better results at SFC values of 60% and 40% (Fig. 5). This can be explained by considering that the attenuation of light is function of the concentration of crystallized material and that the level of attenuation is affected by the radiation wavelength. In particular, the NIR wavelength provides significantly higher accuracy than any visible wavelength for high values of SFC (80%). This can be explained by the fact that, for high values of SFC, the sample becomes opaque and the NIR radiation is characterized by higher optical transmittance than at visible wavelengths. The yellow wavelength (590 nm) provides higher accuracy than the other visible wavelengths for low and average values of SFC (20% - 60%). This can be related to the color of samples which is transparent when in a liquid state and yellowish as crystallization takes place.

Repeatability tests were carried out to investigate the differences in the calculated thermogram with multiple measurements on the same sample. A subset of four samples from the full set presented in Table 1 was characterized, and for each sample five measurements were carried out in sequence. After each measurement, the sample was removed from the sensor and the glass slide was cleaned. The deviation in $T_{90\%,COOLING}$ and $T_{90\%,HEATING}$ was measured for each sample and used to calculate the deviation in the estimated parameters $T_{10\%,DSC}$ and $T_{90\%,DSC}$. The average deviations for the subset of four samples $\Delta T_{10\%,DSC}$ and $\Delta T_{90\%,DSC}$ are presented in Table 5. All the wavelengths investigated were characterized by

high repeatability and maximum deviations that were never higher than 3.3 °C, while the yellow LED (590 nm) and the NIR LED (880 nm) were characterized by deviations that were not higher than 1.4 °C.

4. Conclusions

Measurement of SFC in fats and oils is of primary importance for the food industry since this parameter affects several properties of the final product. Herein, the values of SFC estimated using a recently proposed optical technique were compared with reference values obtained by DSC on 16 fats and oils. The estimated accuracy was evaluated using an *ad-hoc* designed sensor system featuring an array of seven LEDs with peak wavelengths in the visible and NIR ranges that is capable of measuring optical attenuation during a thermal cycle. The estimated accuracy was high for all wavelengths investigated, and the LEDs at peak wavelengths of 590 nm (yellow) and 880 nm (NIR) provided the best correlation with DSC data.

These results demonstrate the feasibility of accurate optical determination of SFC in oils and fats using a limited number of wavelengths. Such measurements can be easily implemented using a portable instrument with inexpensive electronics, which has benefits in terms of low costs and short analysis time. The proposed technique can be a good alternative to reference laboratory analysis (pNMR and DSC), especially for small production centers that cannot afford an internal laboratory for quality analysis. To compete with the reference techniques, however, additional tests are needed on samples characterized by a wider range of SFC. Future investigations will be carried out on a greater number of samples with the use of machine learning algorithms to estimate SFC with higher accuracy.

ACKNOWLEDGMENTS

The authors would like to thank Dr. M. Vanzini for support in providing samples.

References

[1] Dos Santos, M.T., Gerbaud, V., Le Roux, G.A.C., Solid fat content of vegetable oils and simulation of interesterification reaction: Predictions from thermodynamic approach, *Journal of Food Engineering*, 2014, *126*, 198-205.

[2] Flöter, E., The role of physical properties data in product development, *European Journal of Lipid Science and Technology*, 2009, 111, 219-226.

[3] BS EN ISO 8292-2 : 2010 BSI Standards Publication Animal and vegetable fats and oils — Determination of solid fat content by pulsed NMR, 2010.

[4] Leung, H.K., Anderson, G.R., Norr, P.J., Rapid determination of total and solid fat contents in chocolate products by pulsed nuclear magnetic resonance. *Journal of Food Science*, 1985, *50* (4), 942-945.

[5] Márquez, A.L., Pérez, M.P., Wagner, J.R., Solid fat content estimation by differential scanning calorimetry: prior treatment and proposed correction, *Journal of the American Oil Chemists' Society*, 2013, *90* (4), 467-473.

[6] Chiavaro, E., Differential Scanning Calorimetry: applications in fat and oil technology. CRC Press, 2015.

[7] van de Voort, F.R., Memon, K.P., Sedman, J., Ismail, A.A., Determination of Solid Fat Index by Fourier Transform Infrared Spectroscopy, *Journal of the American Oil Chemists' Society*, 1996, 73 (4), 411-416.

[8] Singh, A.P., McClements, D.J., Marangoni, A.G., Solid fat content determination by ultrasonic velocimetry, *Food Research International*, 2004, 37, 545-555.

[9] Grossi, M., Lanzoni, M., Pompei, A., Lazzarini, R., Matteuzzi, D., Riccò, B., A portable biosensor system for bacterial concentration measurements in cow's raw milk, *Proceedings of the 4th IEEE International Workshop on Advances in Sensors and Interfaces*, 2011, 132-136.

[10] Durante, G., Becari, W., Lima, F.A.S., Peres, E.M., Electrical impedance sensor for real-time detection of bovine milk adulteration, *IEEE Sensors Journal*, 2016, 16 (4), 861-865.

[11] Pérez-Esteve, E., Fuentes, A., Grau, R., Fernández-Segovia, I., Masot, R., Alcañiz, M., Barat, J.M., Use of impedance spectroscopy for predicting freshness of sea bream (*Sparus aurata*), *Food Control*, 2014, 35, 360-365.

[12] Grossi, M., Lanzoni, M., Lazzarini, R., Riccò, B., Automatic ice-cream characterization by impedance measurements for optimal machine setting, *Measurement*, 2012, 45, 1747-1754.

[13] Grossi, M., Lazzarini, R., Lanzoni, M., Riccò, B., A novel technique to control ice cream freezing by electrical characteristics analysis, *Journal of Food Engineering*, 2011, 106, 347-354.

[14] Magwili, G.V., Cruz, F.R.G., De Pedro, R.A.C., Evangelista, R.L.C., Icaro, K.P.G., Villarosa, K.A., Non-invasive Moisture Content Prediction and Characterization of Chicken Meat Freshness by Bioelectrical Impedance Spectroscopy, *IEEE 11th International Conference on Humanoid, Nanotechnology, Information Technology, Communication and Control, Environment, and Management (HNICEM)*, 2019, 1-5.

[15] Mignani, A.G., Ciaccheri, L., Mencaglia, A.A., Tuccio, L., Agati, G., Application of a LED-based reflectance sensor for the assessing in situ the licopene content of tomatoes (Lycopersicon esculentum Mill.), *Sensing for Agriculture and Food Quality and Safety VII*. 2015, 9488, International Society for Optics and Photonics.

[16] Liang, P.S., Park, T.S., Yoon, J.Y., Rapid and reagentless detection of microbial contamination within meat utilizing a smartphone-based biosensor, *Scientific Reports*, 2014, 4, 1-8.

[17] Grossi, M., Di Lecce, G., Gallina Toschi, T., Riccò, B., Fast and accurate determination of olive oil acidity by electrochemical impedance spectroscopy, *IEEE Sensors Journal*, 2014, 14 (9), 2947-2954.

[18] Grossi, M., Di Lecce, G., Gallina Toschi, T., Riccò, B., A novel electrochemical method for olive oil acidity determination, *Microelectronics Journal*, 2014, 45, 1701-1707.

[19] Grossi, M., Di Lecce, G., Arru, M., Gallina Toschi, T., Riccò, B., An opto-electronic system for in-situ determination of peroxide value and total phenol content in olive oil, *Journal of Food Engineering*, 2015, 146, 1-7.

[20] Das, A.J., Wahi, A., Kothari, I., Raskar, R., Ultra-portable, wireless smartphone spectrometer for rapid, non-destructive testing of fruit ripeness, *Scientific Reports*, 2016, 6, 1-8.

[21] Wang, M., Huyan, Z., Jing, B., Mao, X., Yu, X., Analysis of edible oil oxidation based on changes in the electrical conductivity of the extracted aqueous phase, *European Journal of Lipid Science and Technology*, 2019, 121 (5), 1800441.

[22] Yan, J., van Stuijvenberg, L., van Ruth, S.M., Handheld near-infrared spectroscopy for distinction of extra virgin olive oil from other olive oil grades substantiated by compositional data, *European Journal of Lipid Science and Technology*, 2019, 121 (12), 1900031.

[23] Grossi, M., Valli, E., Glicerina, V.T., Rocculi, P., Gallina Toschi, T., Riccò, B., Practical determination of solid fat content in fats and oils by single-wavelength near-infrared analysis, *IEEE Transactions on Instrumentation and Measurement*, 2020, 69 (2), 585-592.

[24] Meagher, L.P., Holroyd, S.E., Illingworth, D., van de Ven, F., Lane, S., At-line near-infrared spectroscopy for prediction of the solid fat content of milk fat from New Zealand butter. *Journal of agricultural and food chemistry*, 2007, *55* (8), 2791-2796.

[25] Anderson, N.M., Walker, P.N., Measuring fat content of ground beef stream using on–line visible/NIR spectroscopy. *Transactions of the ASAE*, 2003, *46* (1), 117-124.

[26] Lopez, C., Briard-Bion, V., Camier, B., Gassi, J.Y., Milk fat thermal properties and solid fat content in emmental cheese: a differential scanning calorimetry study, *Journal of dairy science*, 2006, *89* (8), 2894-2910.

[27] McGoverin, C. M., Clark, A. S. S., Holroyd, S. E., Gordon, K. C., Raman spectroscopic prediction of the solid fat content of New Zealand anhydrous milk fat, *Analytical Methods*, 2009, 1(1), 29-38.

[28] Mehrban, H., Lee, D. H., Moradi, M. H., IlCho, C., Naserkheil, M., Ibáñez-Escriche, N., Predictive performance of genomic selection methods for carcass traits in Hanwoo beef cattle: impacts of the genetic architecture, *Genetics Selection Evolution*, 2017, 49(1), 1-13.

[29] Felisaz, P. F., Colelli, G., Ballante, E., Solazzo, F., Paoletti, M., Germani, G., Santini, F., Deligianni, Bergslandgh N., Monforte, M., Tasca, G., Ricci, E., Bastianello, S., Figini, S., Pichiecchio, A., Texture analysis and machine learning to predict water T2 and fat fraction from non-quantitative MRI of thigh muscles in Facioscapulohumeral muscular dystrophy, *European Journal of Radiology*, 2021, 134, 109460.

[30] Meagher, L. P., Holroyd, S. E., Illingworth, D., van de Ven, F., Lane, S., At-line near-infrared spectroscopy for prediction of the solid fat content of milk fat from New Zealand butter, *Journal of agricultural and food chemistry*, 2007, 55(8), 2791-2796.

[31] Tieko Nassau, R., Guaraldp Gonçalves, L. A, Solid fat content determination: Comparison between pNMR and DSC techniques. 1995, *Grasas y aceites*, 46, 337-343.

[32] Rodrigues, J. C., Nascimento, A. C., Alves, A., Osório, N. M., Pires, A. S., Gusmão, J. H., daFonseca M.M.R, Ferreira-Dias, Calibration of near infrared spectroscopy for solid fat content of fat blends analysis using nuclear magnetic resonance data. *Analytica chimica acta*, 2005, 544 (1-2), 213-218.

[33] Walker, R. C., Bosin, W. A., Comparison of SFI, DSC and NMR methods for determining solid liquid ratios in fats. *Journal of the American Oil Chemists' Society*, 1971, 48(2), 50-53.

[34] Lambelet, P., Comparison of N.M.R. and D.S.C. Methods for Determining Solid Content of Fats: Application to Cocoa Butter and Its Admixtures with Milk Fat, 1983, LWT, 16, 200–202.

[35] Shen, Z., Birkett, A., Augustin, M. A., Dungey, S., Versteeg, C., Melting behavior of blends of milk fat with hydrogenated coconut and cottonseed oils. *Journal of the American Oil Chemists' Society*, 2001, 78(4), 387-394.

[36] Dhaygude, V., Soós, A., Zeke, I., Somogyi, L., Comparison Between Static and Dynamic Analyses of the Solid Fat Content of Coconut Oil. *Hungarian Journal of Industry and Chemistry*, 2018, 46(2), 33-36.

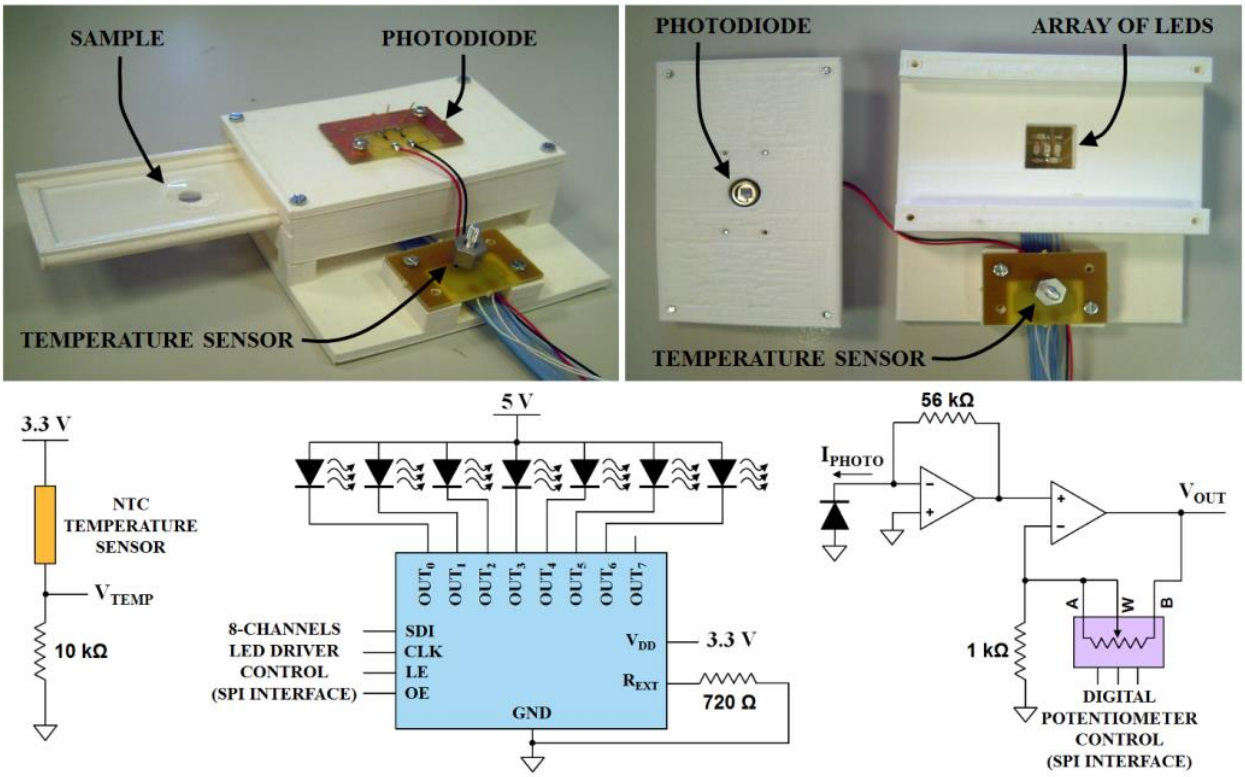

Fig. 1 Photographs of the sensor system and electrical scheme of the conditioning circuits used for the optical measurements.

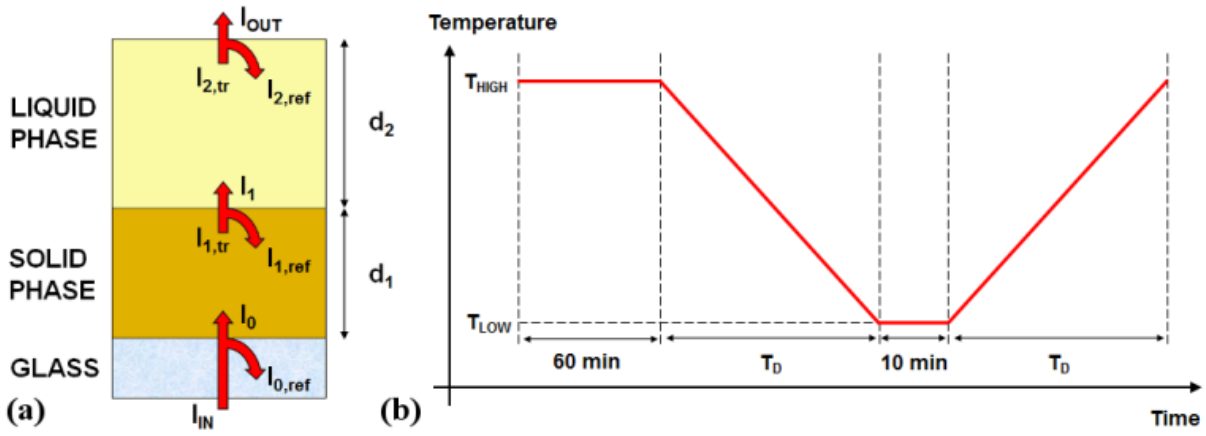

Fig. 2 Optical model of the sample under test (a) and thermal cycle used for the optical measurements (b).

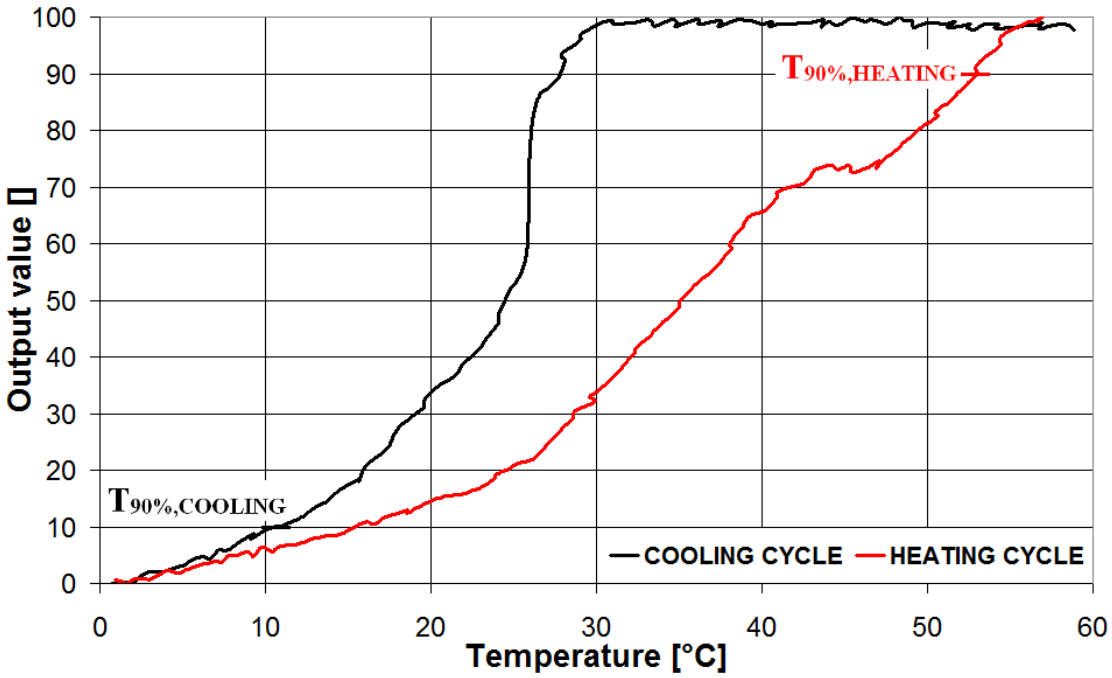

Fig. 3 Measured data during the heating and cooling cycles in the case of IR radiation and sample 8 of Table 1.

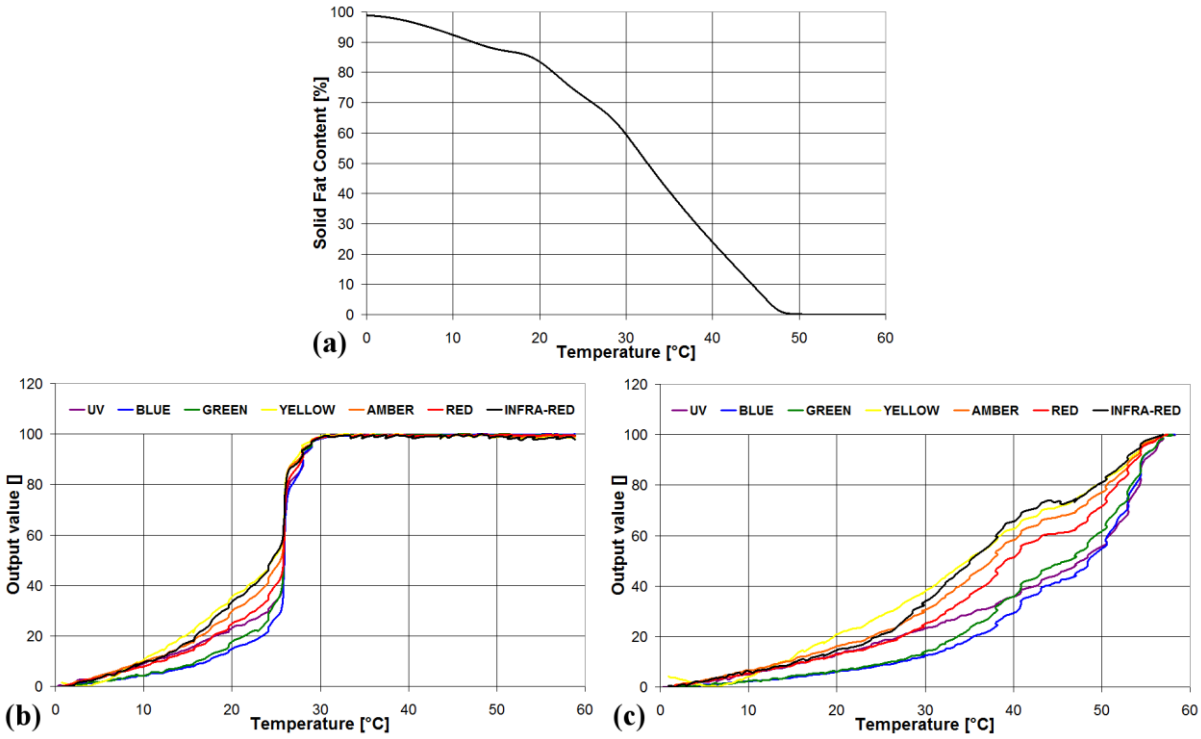

Fig. 4 Typical thermogram curve obtained by DSC (a) and measured optical data *vs* temperature in the case of cooling (b) and heating cycle (c).

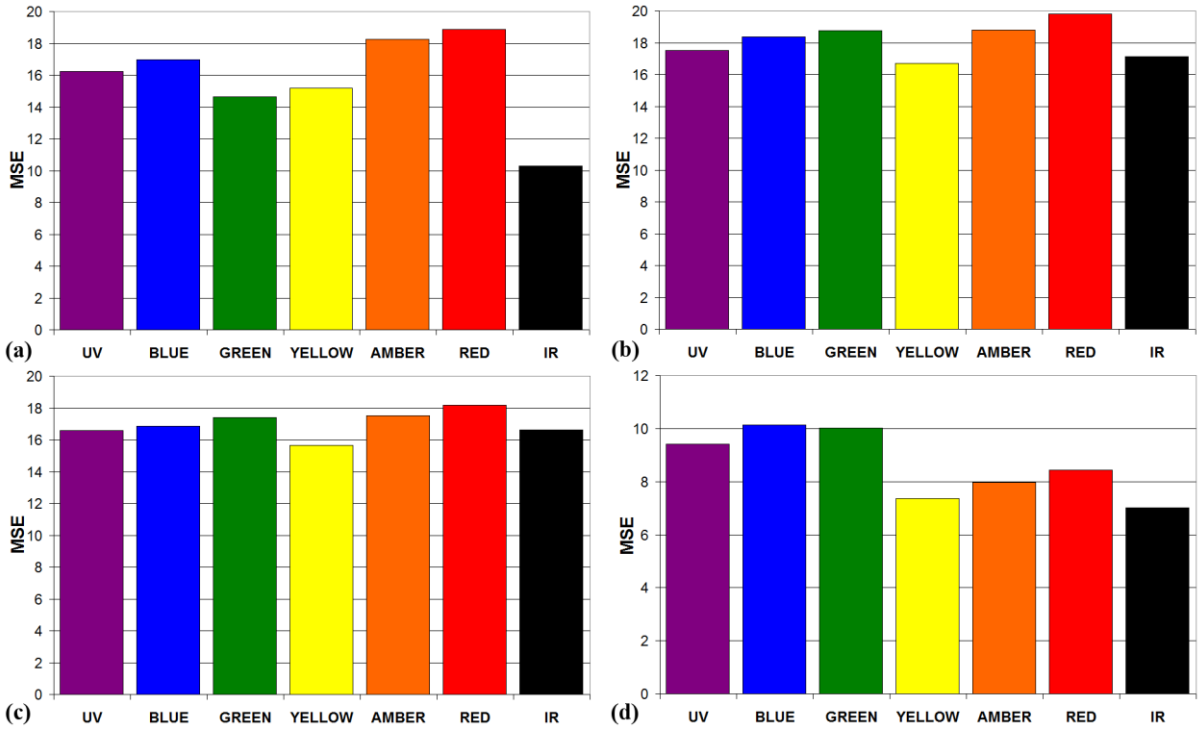

Fig. 5 Histograms for the mean squared error (MSE) obtained for SFC values of 80% (a), 60% (b), 40% (c) and 20% (d).

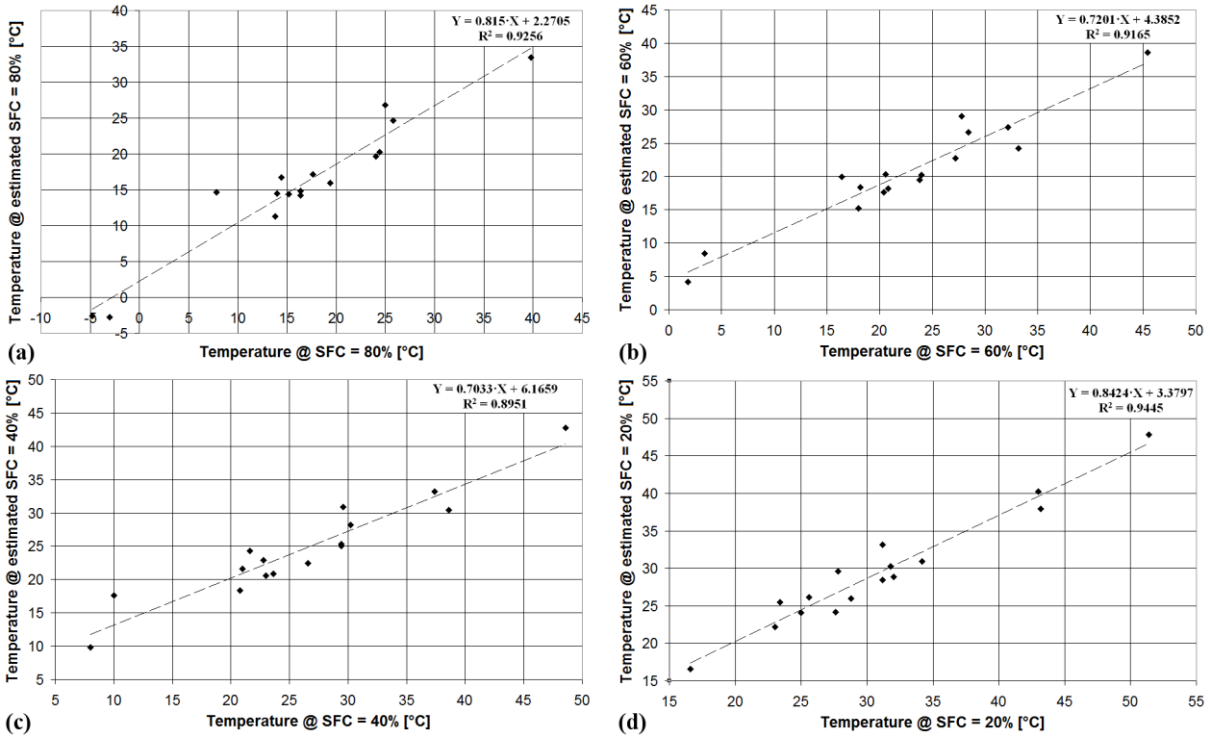

Fig. 6 Scatter plots of the temperature estimated with the proposed method (IR LED) *vs* the temperature determined by DSC in the case of SFC values of 80% (a), 60% (b), 40% (c) and 20% (d).

Table 1 Description of the vegetable oils and fats used in the experiments.

Sample number	Description of the vegetable oils and fats
1	Cocoa butter
2	Refined coconut oil
3	Fractionated coconut oil
4	Blends between fractionated coconut oil and refined coconut oil (50-50, % w/w)
5	Coconut oil
6	Unknown blends of different fats
7	Refined coconut oil
8	Shea butter
9	Monofractionated palm oil
10	Hydrogenated palm oil
11	Refined palm oil
12	Palm kernel oil
13	Hydrogenated soybean oil
14	Blends between hydrogenated soybean oil and refined coconut oil (25-75,% w/w)
15	Blends between hydrogenated soybean oil and refined coconut oil (50-50,% w/w)
16	Blends between hydrogenated soybean oil and refined coconut oil (75-25,% w/w)

Table 2 Values of $T_{90\%,COOLING}$ ($T_{90\%,C}$) and $T_{90\%,HEATING}$ ($T_{90\%,H}$) extracted from the optical thermogram.

Sample number	**λ = 395 nm**		**λ = 468 nm**		**λ = 523 nm**		**λ = 590 nm**		**λ = 610 nm**		**λ = 630 nm**		**λ = 880 nm**	
	$T_{90\%,C}$	$T_{90\%,H}$	$T_{90\%,C}$	$T_{90\%,H}$	$T_{90\%,C}$	$T_{90\%,H}$	$T_{90\%,C}$	$T_{90\%,H}$	$T_{90\%,C}$	$T_{90\%,H}$	$T_{90\%,C}$	$T_{90\%,H}$	$T_{90\%,C}$	$T_{90\%,H}$
1	8.12	31.25	9.17	30.99	9.28	30.99	8.40	30.39	8.61	30.31	9.70	30.30	9.15	30.11
2	7.81	28.60	8.01	28.57	7.74	28.56	7.70	28.33	7.83	28.22	7.98	28.23	7.64	28.09
3	16.08	36.51	17.01	36.88	16.38	36.98	11.63	36.43	14.81	36.44	15.53	36.44	15.58	36.32
4	11.59	33.13	11.36	32.60	11.14	32.66	10.43	32.60	10.80	32.60	10.97	32.60	10.79	32.60
5	10.09	28.66	9.39	28.87	9.83	28.81	8.71	28.66	9.20	28.46	8.76	28.55	7.19	28.28
6	10.63	52.80	15.68	52.80	12.85	52.80	8.86	52.12	9.14	52.11	10.14	52.26	8.19	51.14
7	14.96	32.86	15.10	33.09	15.03	32.95	14.13	32.65	14.65	32.63	14.64	32.65	14.18	32.62
8	10.70	54.91	17.38	54.64	16.19	54.58	9.87	52.97	10.21	53.35	12.13	53.88	10.55	52.99
9	−4.34	31.05	−1.79	30.91	−2.54	30.77	−4.93	27.78	−5.15	26.80	−4.03	27.43	−4.17	25.61
10	18.15	57.93	26.35	57.95	24.37	57.94	17.53	58.02	15.16	58.18	16.62	58.11	19.39	58.19
11	−6.15	49.86	−2.02	49.75	-2.99	49.57	−5.97	48.69	−6.20	48.45	−4.78	48.53	−5.01	47.39
12	9.16	30.89	10.24	30.81	9.95	30.83	8.57	30.51	8.65	30.29	8.64	30.60	8.32	30.59
13	8.48	42.18	11.81	42.15	10.38	42.02	8.50	40.43	8.48	40.44	9.39	40.49	6.94	40.26
14	5.71	27.64	5.76	27.51	5.63	27.45	5.62	27.02	5.64	26.91	5.67	27.00	5.29	26.82
15	9.03	35.64	10.71	35.53	10.21	35.21	8.33	33.01	8.37	33.04	9.04	33.15	7.31	30.66
16	8.18	39.55	11.69	39.25	10.75	39.15	8.34	37.87	8.39	37.89	9.28	37.99	7.22	37.83

Table 3 Linear regression coefficients for the different wavelengths investigated

λ (nm)	β_1	β_2	β_3	β_4	β_5	β_6
395	0.5159	1.6149	$-6.858 \cdot 10^{-2}$	2.4847	0.3572	0.7278
468	11.664	1.6300	-0.4636	4.9788	0.3578	0.6418
523	8.4734	1.6436	-0.3534	4.2825	0.3466	0.6710
590	0.2281	1.7231	$-5.164 \cdot 10^{-2}$	3.2196	0.3196	0.7429
610	-2.0256	1.6641	0.0131	3.4936	0.2722	0.7459
630	-0.3745	1.7109	$-7.291 \cdot 10^{-2}$	3.6105	0.2871	0.7317
880	1.8421	1.7403	-0.1083	4.2427	0.2456	0.7398

Table 4 Regression line equation for the temperature estimated from optical and DSC data in the case of SFC values of 80%, 60%, 40% and 20% and the corresponding coefficient of determination (R^2) in the case of all wavelengths investigated.

λ (nm)		**T @ SFC = 80% (°C)**	**T @ SFC = 60% (°C)**	**T @ SFC = 40% (°C)**	**T @ SFC = 20% (°C)**
395	*Regression equation*	y = 0.7676x + 3.0588	y = 0.7022x + 4.7899	y = 0.6891x + 6.538	y = 0.8098x + 4.3885
	R^2	0.8703	0.9237	0.9067	0.9111
468	*Regression equation*	y = 0.7531x + 3.3007	y = 0.6914x + 5.0344	y = 0.6834x + 6.6885	y = 0.8027x + 4.6094
	R^2	0.8663	0.9190	0.9066	0.9003
523	*Regression equation*	y = 0.7707x + 3.0077	y = 0.6937x + 4.9826	y = 0.6828x + 6.7036	y = 0.8047x + 4.5473
	R^2	0.8883	0.9111	0.8969	0.9020
590	*Regression equation*	y = 0.7692x + 3.0333	y = 0.7077x + 4.665	y = 0.6989x + 6.2792	y = 0.8336x + 3.6514
	R^2	0.8824	0.9327	0.9154	0.9407
610	*Regression equation*	y = 0.7495x + 3.3604	y = 0.6927x + 5.0042	y = 0.6842x + 6.6657	y = 0.8243x + 3.9377
	R^2	0.8522	0.9108	0.8936	0.9327
630	*Regression equation*	y = 0.742x + 3.4857	y = 0.6845x + 5.1894	y = 0.6782x + 6.8237	y = 0.8193x + 4.0927
	R^2	0.8473	0.9011	0.8868	0.9258
880	*Regression equation*	y = 0.815x + 2.2705	y = 0.7201x + 4.3852	y = 0.7033x + 6.1659	y = 0.8424x + 3.3797
	R^2	0.9256	0.9165	0.8951	0.9445

Table 5 Average deviation for the estimated parameters $\Delta T_{10\%,DSC}$ and $\Delta T_{90\%,DSC}$ for all the wavelengths investigated

λ (nm)	**$\Delta T_{90\%,DSC}$ (°C)**	**$\Delta T_{10\%,DSC}$ (°C)**
395	3.214	1.421
468	1.029	1.131
523	1.077	0.801
590	1.319	0.854
610	2.984	1.156
630	2.191	1.095
880	1.398	0.917